doi:10.1093/plphys/kiab159 PLANT PHYSIOLOGY 2021: 187: 618–631

Plant Physiology®

Breakthrough Tech

Sensing stress responses in potato with whole-plant redox imaging

Matanel Hipsch [1], Nardy Lampl [1], Einat Zelinger [2], Orel Barda,[1] Daniel Waiger [2] and Shilo Rosenwasser [1,*,†]

1 The Robert H. Smith Institute of Plant Sciences and Genetics in Agriculture, The Hebrew University of Jerusalem, Rehovot 7610000, Israel
2 Center for Scientific Imaging Core Facility, The Robert H. Smith Faculty of Agriculture, Food & Environment, The Hebrew University of Jerusalem, Rehovot 7610001, Israel

*Author for communication: shilo.rosenwaser@mail.huji.ac.il
†Senior author.
The author responsible for distribution of materials integral to the findings presented in this article in accordance with the policy described in the Instructions for Author (https://academic.oup.com/plphys/pages/general-instructions) is: Shilo Rosenwasser (shilo.rosenwaser@mail.huji.ac.il).

Abstract

Environmental stresses are among the major factors that limit crop productivity and plant growth. Various nondestructive approaches for monitoring plant stress states have been developed. However, early sensing of the initial biochemical events during stress responses remains a significant challenge. In this work, we established whole-plant redox imaging using potato (*Solanum tuberosum*) plants expressing a chloroplast-targeted redox-sensitive green fluorescence protein 2 (roGFP2), which reports the glutathione redox potential (E_{GSH}). Ratiometric imaging analysis demonstrated the probe response to redox perturbations induced by H_2O_2, DTT, or a GSH biosynthesis inhibitor. We mapped alterations in the chloroplast E_{GSH} under several stress conditions including, high-light (HL), cold, and drought. An extremely high increase in chloroplast E_{GSH} was observed under the combination of HL and low temperatures, conditions that specifically induce PSI photoinhibition. Intriguingly, we noted a higher reduced state in newly developed compared with mature leaves under steady-state and stress conditions, suggesting a graded stress sensitivity as part of the plant strategies for coping with stress. The presented observations suggest that whole-plant redox imaging can serve as a powerful tool for the basic understanding of plant stress responses and applied agricultural research, such as toward improving phenotyping capabilities in breeding programs and early detection of stress responses in the field.

Introduction

Crop plants live in highly dynamic environments, in which abiotic stresses, such as salinity, drought, high temperature, and high light (HL), are thought to be the major constraints of crop production and ultimately of food security (Fahad et al., 2017). Continuous exposure to moderate stress levels or even to suboptimal growth conditions interrupts plant homeostasis and results in constant energy loss due to resource diversion toward the activation of defense and acclimation mechanisms (Zhu, 2016).

As a third major food crop, potato (*Solanum tuberosum*) productivity is crucial for worldwide food security (Devaux et al., 2014). Over the past 20 years, there has been a dramatic increase in potato production and demand in Asia, Africa, and Latin America (da FAOSTAT, 2014). The potato tubers are rich sources of carbohydrates and provide essential nutrients, such as dietary fiber, vitamins, minerals, protein, and antioxidants (Burlingame et al., 2009; Bach et al., 2012). Despite the wide distribution and adaptability of the potato plant to various environmental and climatic

Received March 1, 2021. Accepted March 22, 2021. Advance access publication April 6, 2021

conditions, potato productivity is highly affected by environmental conditions (Bohnert, 2007). Even exposure to mild abiotic stresses such as drought and heat, as prevalent in potato-growing regions, reduces photosynthesis efficiency, which significantly impacts potato production and quality (Deblonde and Ledent, 2001; George et al., 2017).

In the past few decades, there has been a growing demand for biosensing technologies that allow for dynamic monitoring of crop growth and stress status to support "on-line" decisions ensuring the long-term sustainability of crop productivity. A range of technologies has been successfully implemented to nondestructively perceive information regarding the physiological status of plants, such as chlorophyll fluorescence imaging to detect photosynthetic activity (Wang et al., 2018), thermal imaging to estimate stomatal conductance and transpiration (Costa et al., 2013), multispectral imaging to evaluate crop water and nutrient status (Wang et al., 2018), and terahertz spectroscopy to detect plant drought stress responses (Born et al., 2014). However, technologies for early detection of the cellular biochemical signals involved in sensing and processing of environmental information regarding abiotic and biotic stress are still lacking, mainly due to the destructive nature of common biochemical methods.

Stress-induced alterations in plant metabolism are typically accompanied by modifications in the levels of reactive oxygen species (ROS), which can differ in their chemical identity and subcellular localization (Foyer and Noctor, 2003; Gadjev et al., 2006; Miller et al., 2010; Møller and Sweetlove, 2010). Thus, increased ROS or oxidized metabolite levels, as well as the ROS-induced gene products, are common biomarkers for stress responses. Imaging and detection of ROS in live cells have been achieved using various fluorescent or dyes, such as 3,3′-diaminobenzidine (DAB), Amplex Red, and 2′,7′-dichlorodihydrofluorescein diacetate (H_2DCFDA; Halliwell and Whiteman, 2004; Van Breusegem et al., 2008; Gao and Zhang, 2008; Zhang et al., 2009; Fichman et al., 2019, 2020). A new type of nano-sensor probes, based on single-walled carbon nanotubes, was shown to enable real-time spatiotemporal monitoring of H_2O_2 within plants (Lew et al., 2020; Wu et al., 2020). While these probes can be easily implemented in a wide range of plants, and provide valuable information on alterations in ROS metabolism on the whole-plant level, they require the incorporation of the probes to plant tissues, making it challenging to investigate redox alterations on the whole-plant level over long, physiologically relevant time periods.

Genetically encoded redox-sensitive green fluorescent proteins (roGFPs) have been developed and used as biosensors in various model systems. In vitro characterization of roGFP activity pointed to its predominant interaction with the cellular GSH pool through the mediation of glutaredoxin activities (GRXs, Meyer et al., 2007). These in vitro observations were corroborated by the substantial in vivo oxidation of cytosol-targeted roGFP recorded upon external application of L-buthionine (S,R)-sulfoximine (BSO), a glutathione biosynthesis inhibitor that specifically inhibits γ-glutamylcysteine synthetase (GSH1, Meyer et al., 2007). In agreement, a higher roGFP oxidation state was measured in Arabidopsis (*Arabidopsis thaliana*) plant with aberrant GSH biosynthesis and reduction pathways (Meyer et al., 2007; Rosenwasser et al., 2010). The linkage between roGFP and the GSH pool suggests that endogenous GRXs mediate the interaction between GSH and roGFP and point to the possibility of in vivo GSH redox potential (E_{GSH}) probing by roGFP. Its mechanism of action is based on two engineered surface-exposed cysteine residues, which form an intramolecular disulfide bridge that impacts its fluorescence characteristics. Due to their ratiometric nature, high sensitivity, reversibility, and insensitivity to pH alterations in the physiological range, roGFP-based redox sensors are powerful tools for investigating redox dynamics in subcellular compartments at high spatiotemporal resolution (Dooley et al., 2004; Hanson et al., 2004; Jiang et al., 2006b; Gutscher et al., 2008; Meyer and Dick, 2010; Albrecht et al., 2011; Bratt et al., 2016; Schwarzländer et al., 2016; Nietzel et al., 2019; Ugalde et al., 2020). Their reversibility enables the monitoring of their redox state at multiple points over time without damaging the tissue. Notably, as the roGFP redox state is regulated by counteracting oxidative and reductive reactions, it reflects the transmission of redox signals, leading to modulation of the redox state of native redox-sensitive proteins as part of plant stress acclimation (Meyer, 2008; Rosenwasser et al., 2014).

Despite the great potential in using genetically encoded biosensors to detect stress responses in plants, current approaches for measuring roGFP-based signals are mainly based on confocal microscopy and plate readers, which are suitable for plant pieces or small model plants, but not for intact plants grown in soil. Only recently, whole-plant fluorescence imaging has been demonstrated in *Arabidopsis* plants expressing genetically encoded biosensors (Fichman and Mittler, 2021; Haber et al., 2021) but has not been applied to crop plants grown in soil. The global importance of potato crop and the availability of highly efficient transformation protocols render potato an ideal platform for investigating genetically encoded biosensor performance in crop plants.

In this work, potato plants expressing chloroplast-targeted roGFP2 were generated and subjected to whole-plant roGFP ratiometric imaging analysis using a highly sensitive in vivo imaging system. The experimental setup enabled detection of in planta redox modification in response to several abiotic stress conditions that mimicked natural field conditions. The presented data demonstrate that whole-plant imaging of roGFP-expressing plants allowed for spatially resolved mapping of stress-induced redox perturbations over long periods. These results may have important implications on phenotyping capacities in large-scale breeding projects and on

capabilities to detect stress conditions in crop plants under field conditions.

Results and discussion

Generation of potato plants expressing a genetically encoded redox probe

The roGFP probe allows for quantitative, real-time readout of E_{GSH} in living cells (Meyer et al., 2007; Albrecht et al., 2011). To enable the monitoring of temporal alterations in the chloroplastic E_{GSH} (chl-E_{GSH}) on the whole-plant level, *Agrobacterium*-mediated genetic transformation was performed to obtain potato plants cv *Desiree* expressing the roGFP2 probe in the chloroplast (chl-roGFP2, Supplemental Figure S1). Chloroplast targeting was achieved by using the *Arabidopsis* 2-Cys peroxiredoxin A signal peptide, which is targeted to the chloroplast stroma (König et al., 2002), as verified by the overlap of the chl-roGFP2 and the chlorophyll fluorescence signals (Figure 1, A). No phenotypic differences between several independent lines expressing the roGFP2 probe and wild type were observed; the line with the highest fluorescence intensity and lowest variability in roGFP2 signals between individual plants was selected for subsequent experiments (Supplemental Figure S2). roGFP signal silencing, a phenomenon frequently reported for plant protein-based biosensors and which has been observed to increase over generations (Schwarzländer et al., 2016; Exposito-Rodriguez et al., 2017), was not detected, presumably since lines were vegetatively propagated, either from cuttings or tubers. Confocal microscopy analysis was used to validate the in vivo probe redox sensitivity, which was determined via ratiometric images derived from the division of the emitted fluorescence due to excitation at 405 nm by the emitted fluorescence following 488 nm excitation ($R_{405/488}$). These ratios, which indicate the roGFP2 oxidation state (Dooley et al., 2004; Hanson et al., 2004), were calculated for plants in a steady state and following treatment with H_2O_2 or DTT. As shown in Figure 1, B and C, an increase and decrease in excitation ratios were observed following treatment with H_2O_2 and DTT, respectively. Relatively low ratio values were recorded under steady-state conditions, indicating a highly reduced chl-roGFP2 state. These results are consistent with probe characteristics previously observed in plant cells (Schwarzländer et al., 2008).

In vivo redox imaging of potato biosensor plants

To establish in vivo quantitative mapping of the chl-E_{GSH} on a whole-plant level, roGFP2 probe emission at 515 nm was recorded from intact plants grown in soil using a highly sensitive in vivo imaging system (see the "Materials and methods" section), following excitation at 405 and 465nm with light-emitting diodes (LEDs). To explore the ability of this setup to provide reliable information on in planta chloroplast-specific redox alterations without tissue autofluorescence perturbations, the fluorescent signal measured in plants expressing the roGFP2 probe was compared with that measured in wild-type plants. As shown in Figure 1, D, a clear separation between the pixel intensity histograms of roGFP2-expressing versus wild-type lines was observed following excitation at 405 and 465 nm, demonstrating an intense roGFP2 signal in the former lines. The measured autofluorescence signals were 2.2% and 9.6% of the total fluorescence signals, emitted from roGFP2-expressing plants, following excitation at 465 and 405 nm, respectively (Figure 1, D and Supplemental Figure S3). In all subsequent experiments, autofluorescence values obtained from wild-type plants exposed to the same conditions as roGFP-expressing lines were used for background correction (see the "Materials and methods" section). Correction for background values is also highly important under specific stress conditions that increase autofluorescence, especially in the 405 nm- excitation range (Rosenwasser et al., 2010).

To monitor the in planta response to redox changes, 2.5-week-old chl-roGFP2-expressing plants grown from cuttings were imaged under steady-state conditions and following the application of H_2O_2 or DTT. While some variability in absolute roGFP fluorescence intensities was observed across different leaves, pixel-by-pixel $R_{405/465}$ images provided informative false-color images (Figure 1, E). Upon H_2O_2 treatment, an increase in 405 nm-excited fluorescence and a decrease in 465 nm-excited fluorescence were observed, demonstrating probe oxidation. Conversely, DTT treatment resulted in probe reduction, as demonstrated by the less intense signal following 405 nm excitation and increased brightness following 465 nm excitation. Ratiometric images of untreated plants showed the highly reduced chl-E_{GSH} throughout the whole plant. The temporal response of 4–5-week-old plants to oxidative conditions was further assessed by watering of soil-grown chl-roGFP2-expressing plants with 50 mL 1 M H_2O_2. Ratiometric images demonstrated an increase in the chl-roGFP2 oxidation state, mainly in mature leaves, which became saturated after 12 min of exposure, and was then followed by reduction, reaching a steady-state level after 27 min (Figure 1, F, Supplemental Movie S1, and Supplemental Figure S4).

Previous experiments using confocal imaging showed that the application of BSO to *Arabidopsis* roots led to substantial oxidation of cytosol-targeted roGFP (Meyer et al., 2007). Hence, to further demonstrate that the whole-plant imaging approach allows for spatially resolved monitoring of redox alterations, we monitored chl-roGFP2 fluorescence signals following depletion of the cellular GSH pool by BSO. Images were obtained daily from 4-week-old plants grown in soil and watered with 2.5 mM BSO. A significant increase in $R_{405/465}$ was observed, starting 1 d after BSO treatment and reaching maximum values ($R_{405/465}$ of 0.3 ± 0.052 compared with 0.1 ± 0.012 recorded from control plants) on the third day of treatment (Figure 2, A–D and Supplemental Figure S5). These observations were further validated using confocal microscopy imaging analysis, which confirmed chloroplast-specific E_{GSH} oxidation (Figure 2, E and F).

Interestingly, under steady-state conditions, newly developed leaves on the higher part of the plant exhibited lower

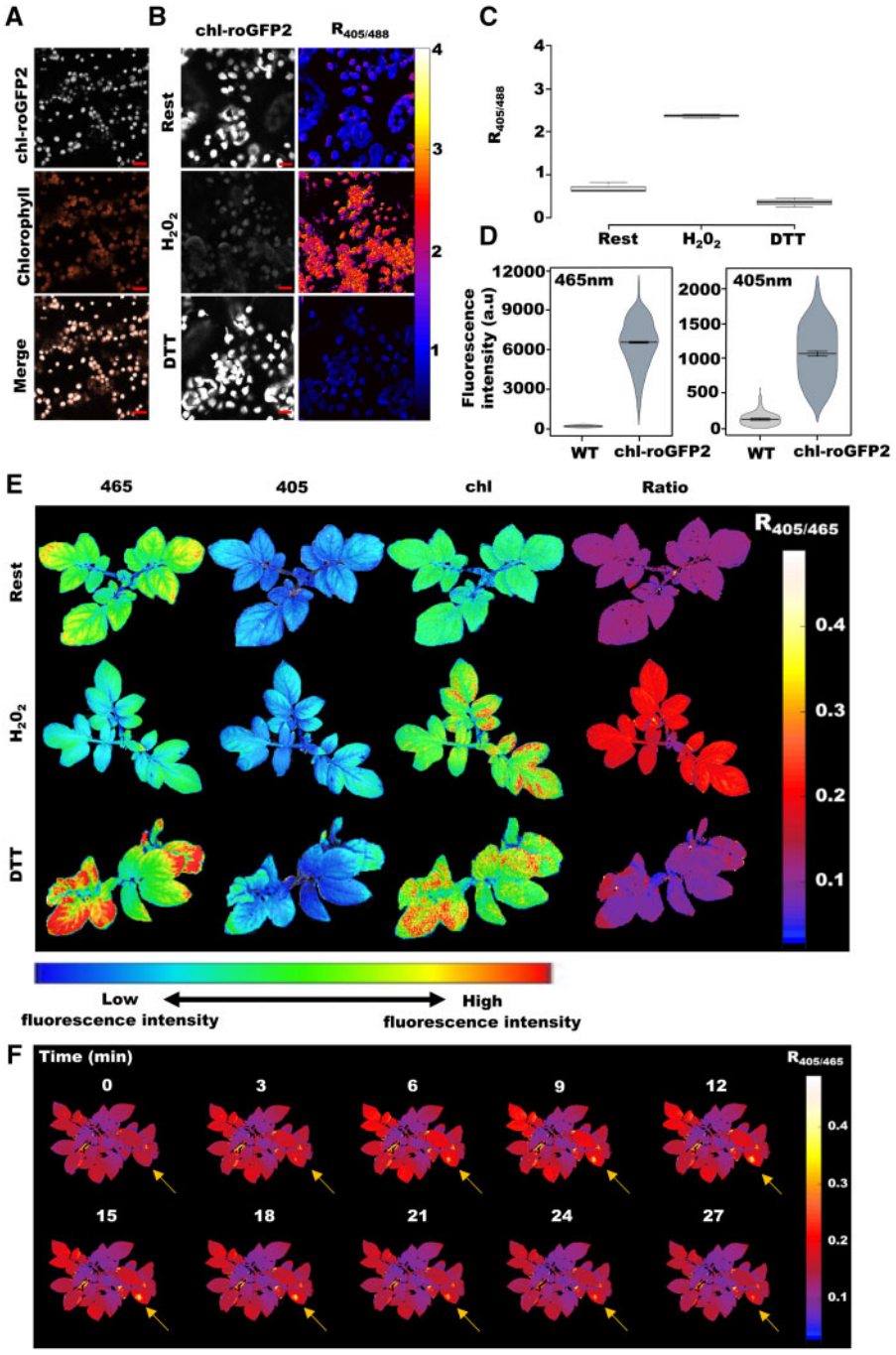

Figure 1 Live imaging of potato plants expressing roGFP2 in chloroplasts. A, Confocal images of chl-roGFP2-expressing potato plants showing (chl-roGFP2 excitation: 488 nm). Red lines indicate 10 μm length. B, Ratiometric confocal images of chloroplasts during rest, fully oxidized (1,000 mM H_2O_2) and fully reduced (100 mM DTT) states are shown. Red lines indicate 10 μm length. C, Quantification of ratiometric images in B presented as box plot ($n = 3$). Center lines show the medians; box limits indicate the 25th and 75th percentiles; whiskers extend 1.5 times the interquartile range from the 25th and 75th percentiles. D, Comparison between the emission intensities detected by whole-plant imaging at 515 nm in WT and roGFP2-expressing plants, following excitation with 465 or 405 nm. The data are summarized as a violin plot reflecting the pixel distribution of a representative plant. E, Fluorescence whole-plant images and ratiometric analysis of chl-roGFP2 signals during rest and under fully oxidized (1,000 mM H_2O_2) and fully reduced (100 mM DTT) conditions. Individual plant images were digitally combined for comparison. F, Whole-plant ratiometric images of potato plant watered with 1 M H_2O_2 and monitored over 27 min. The numbers at the top represent the time from H_2O_2 application. The yellow arrows highlight the oxidation changes of a specific leaf during H_2O_2 treatment. Individual plant images were digitally combined for comparison. A movie visualization is depicted as Supplemental Movie S1.

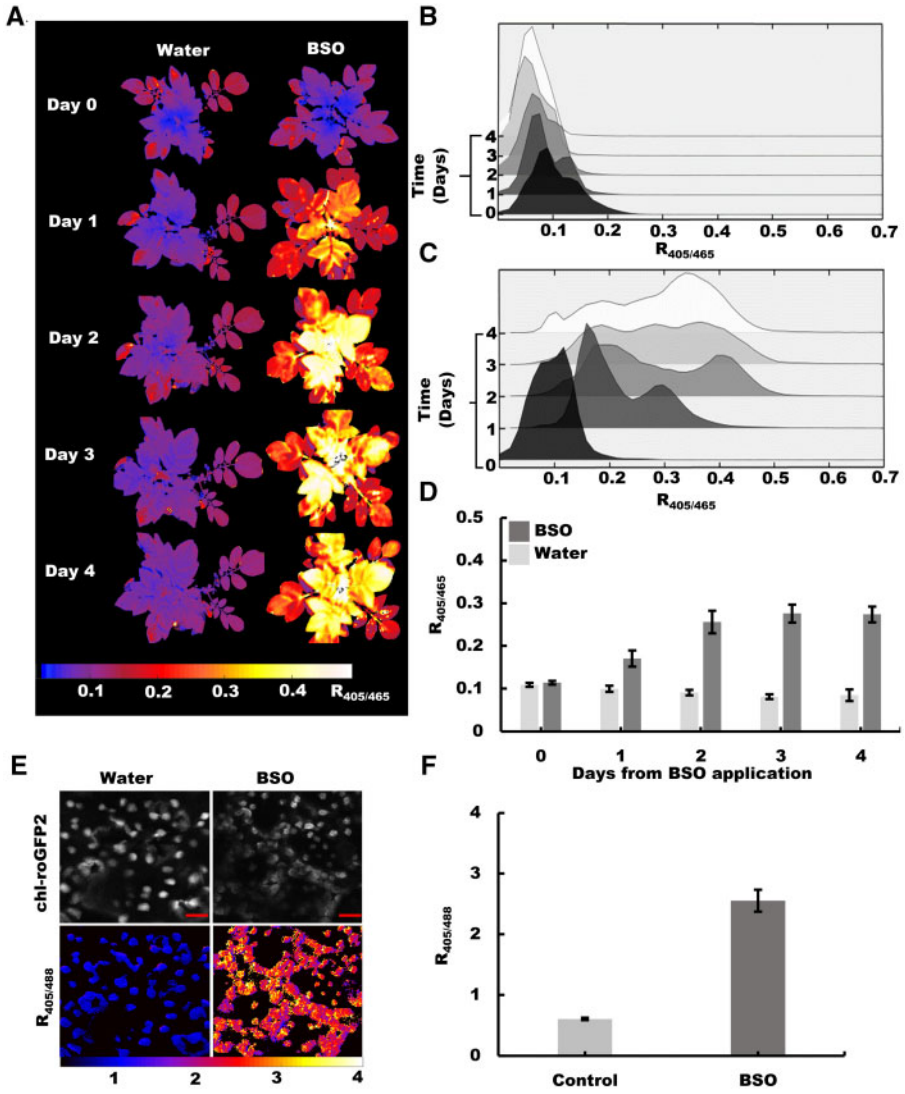

Figure 2 Whole-plant imaging demonstrates chl-roGFP2 oxidation in response to GSH depletion. A, Whole-plant temporal ratiometric images of representative plants irrigated with 2.5 mM Buthionine sulfoximine (BSO) or water, over 4 d. Individual plant images were digitally combined for comparison. B and C, Ridgeline plot showing the pixel distributions of ratio images of a representative plant irrigated with water (B) or BSO (C). D, Quantification of ratio images presented in A. Values represent mean ± SE ($n = 4$). E, Confocal images of chl-roGFP2 (excitation: 488 nm) and ratiometric analysis on the fourth day of treatment. F, Quantification of the ratiometric images presented in E. Values represent mean ± SE ($n = 3$).

$R_{405/465}$ values when compared with lower and mature leaves, suggesting a more reduced state of the E_{GSH} in young leaves (Figure 2, A). Spatial differences were also observed following BSO application, where a higher chl-roGFP2 oxidation state was measured in young leaves (Figure 2, A). However, these observations, which imply the higher sensitivity of young leaves to the inhibition of the de novo synthesis of GSH, can also result from an unequal distribution of BSO among the plant tissue.

To further calibrate the probe's dynamic range by defining $R_{405/465}$ values for the fully oxidized and reduced states, detached leaves were soaked in various H_2O_2 solutions and the redox state was monitored. Treatment of leaves with increasing H_2O_2 concentrations (10–1500 mM) resulted in increased $R_{405/465}$ (Figure 3, A and B and Supplemental Figure S6, A–C). At relatively high H_2O_2 concentrations (750–1000 mM), chl-roGFP2 fluorescence reached saturation ($R_{405/465}$ = 0.49) within 12 min. Notably, these values do not reflect the endogenous H_2O_2 concentrations, which are affected by penetration rates and detoxification activity. Treatment of leaves with 100 mM DTT resulted in a decrease in $R_{405/465}$ (0.09), demonstrating a dynamic range of 5.4 ($R_{405/465}$ for fully oxidized state divided by $R_{405/465}$ for fully reduced state), which is comparable to values determined using confocal microscopy and a plate reader (Schwarzländer et al., 2008; Rosenwasser et al., 2010). Markedly, $R_{405/465}$ values of the fully oxidized or fully reduced chl-roGP2 states in newly developed leaves were

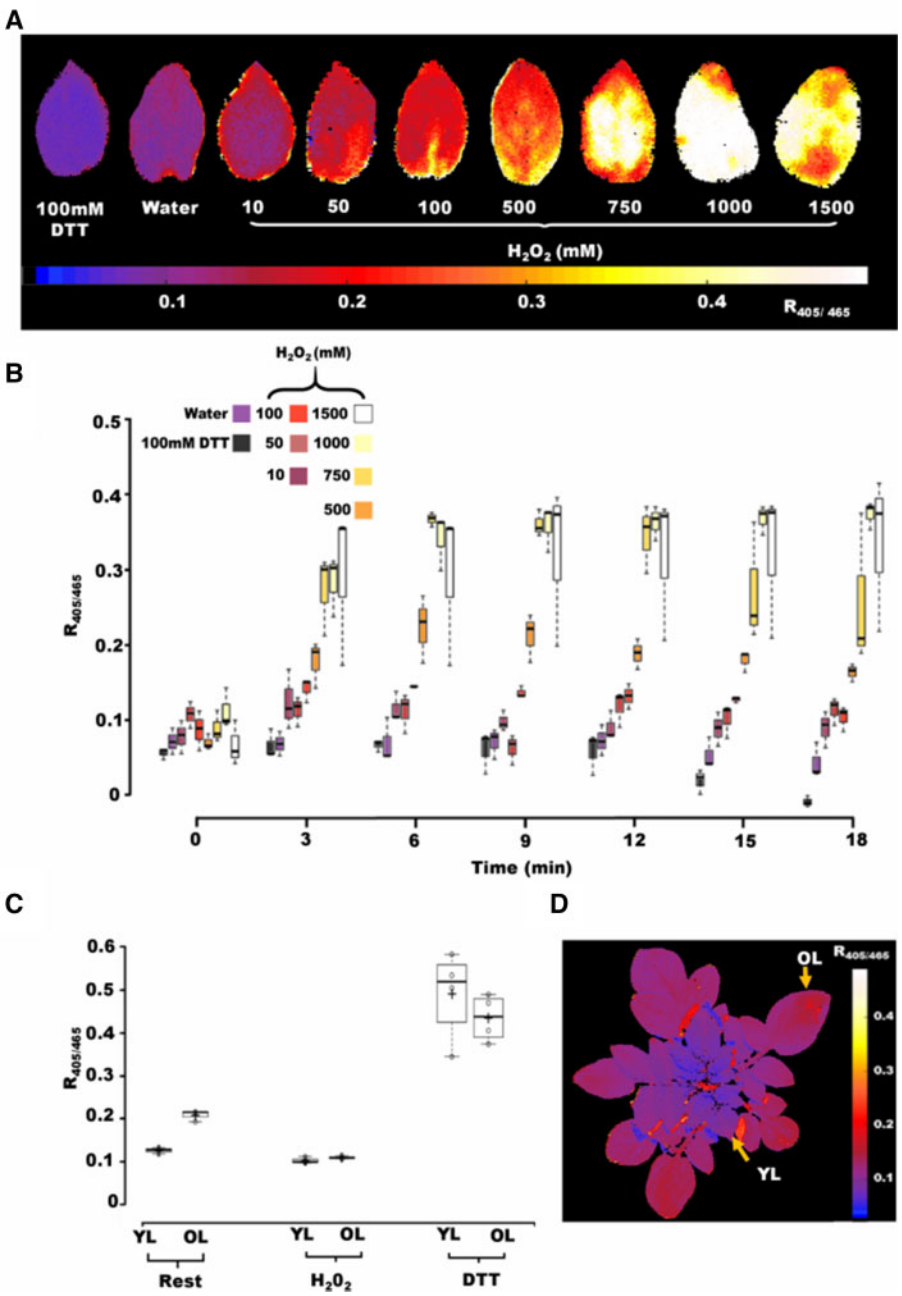

Figure 3 Calibration of chl-roGFP2 dynamic range. Detached leaves from plants expressing the chl-roGFP2 probe were treated with various H_2O_2 concentrations or 100 mM DTT. A, Ratiometric images of representative leaves 12 min after H_2O_2 application or 60 min after applying DTT. Individual plant images were digitally combined for comparison. B, Temporal response of chl-roGFP2 in potato leaves to increasing concentrations of H_2O_2, as evaluated using ratiometric fluorescence imaging and presented as a box plot. Center lines show the medians; box limits indicate the 25th and 75th percentiles; whiskers extend 1.5 times the interquartile range from the 25th and 75th percentiles. C, Comparison between chl-roGFP2 $R_{405/465}$ values of young leaves (YL) to those of old leaves (OL) under rest, fully oxidized (1,000 mM H_2O_2) or fully reduced (100 mM DTT) conditions. The $R_{405/465}$ values are presented as a box plot ($n = 3$). Center lines show the medians and plus signs represent sample means.; box limits indicate the 25th and 75th percentiles; whiskers extend 1.5 times the interquartile range from the 25th and 75th percentiles; open circles represent samples. D, Whole-plant imaging of plants grown under CL conditions (300 μmol photons m^{-2} s^{-1}), highlighting the spatial distribution of redox changes in young versus old leaves.

similar to those observed in mature leaves (Figure 3, C and D), suggesting that the observed differences in steady-state $R_{405/465}$ values indeed reflected differences in chl-roGFP2 oxidation state.

The oxidation degree (OxD) of chl-roGFP2 and chl-E_{GSH} in whole plants under steady-state conditions was then calculated using reference ratio values for fully oxidized and reduced states according to Meyer et al. (2007). The average

OxD values were approximately 25%. Considering a stromal pH of 8, this OxD value would reflect an $E_{GSH} = -346$ mV, which aligns with previous calculations of chloroplastic E_{GSH} under steady-state conditions in *Arabidopsis* plants (Schwarzländer et al., 2008; Rosenwasser et al., 2010). Interestingly, newly developed and mature leaves exhibited an average chl-roGFP2 OxD of 14% and 28%, respectively, demonstrating a deviation of 11 mV between different leaves on the same plant (Figure 3, C).

Daily measurements of chl-E_{GSH} under HL

Potato biosensor plants offer the opportunity to examine the in vivo influence of environmental stress conditions on the chl-E_{GSH} and to examine possible redox differences throughout plants. As the chl-E_{GSH} dynamically responds to changes in light intensities (Haber et al., 2021), we sought to apply the chl-roGFP2 probe to investigate potato plant response to changes in light intensities that mimic the kinetics and light intensities of field conditions. To this end, 4-week-old plants were exposed to the following 16-h light conditions: Constant light (CL)—200 µmol photons m^{-2} s^{-1}, medium-light (ML)—light intensity was gradually increased, reaching a maximum value of 720 µmol photons m^{-2} s^{-1}, followed by a gradual decrease toward the end of the day, or HL—gradual increases in light intensity, up to a maximum value of 1250 µmol photons m^{-2} s^{-1} light (Figure 4). roGFP fluorescence images were taken every 2 h, starting from light onset. As shown in Figure 4, A and B and Supplemental Figure S7, plant exposure to increasing light intensities (ML and HL) resulted in an increased whole-plant chl-roGFP2 oxidation state, reaching maximum values in the middle of the day. Similar oxidation dynamics were observed in plants exposed to ML and HL, with slightly higher oxidation values under the HL treatment. For example, at 8 h from light onset, OxD values of 47 ± 6% and 43 ± 6% were recorded in plants exposed to HL and ML, respectively. Relatively constant chl-roGFP2 OxD, of approximately 30%, was measured throughout the day in plants exposed to CL. The difference in the roGFP2 oxidation state between HL and CL-exposed plants is equivalent to a 10-mV increase in chl-E_{GSH}, in agreement with values obtained in *Arabidopsis* plants under HL conditions (Haber et al., 2021). Return to steady-state values was detected 14 h after light onset, when light intensity was reduced to 200 µmol photons m^{-2} s^{-1}. The inspection of ratiometric images revealed that although a light-induced oxidation response was detected in all plant leaves, mature leaves responded stronger to increasing light intensities than young leaves, with differences of 28% and 10% in chl-roGFP2 OxD between HL and CL conditions 8 h from light onset in old versus young leaves, respectively (Figure 4, A and C). Taken together, these observations demonstrate that spatial heterogeneity and physiological responses of chl-E_{GSH} to light intensity can be nondestructively monitored in crop plants grown in soil. As HL induces H_2O_2 production (Exposito-Rodriguez et al., 2017), the increase in chl-E_{GSH} is likely a reflection of a new balance point between photosynthesis-dependent ROS production and NADPH-dependent glutathione reductase (GR) activity. Notably, as roGFP2 oxidation–reduction dynamics may reflect similar patterns occurring in many redox-regulated metabolic proteins, specifically those regulated by native GRXs (Meyer, 2008; Rosenwasser et al., 2014), it may provide an important readout of stress-induced metabolic alterations.

Profound chl-E_{GSH} oxidation under HL and cold temperatures

Various environmental conditions lead to an imbalance between photosynthesis light absorption and downstream carbon assimilation reactions, resulting in increased plant sensitivity to excess light energy. Specifically, photosystem I (PSI) photo-inactivation was observed in chilled potato leaves exposed to HL, likely due to ROS accumulation (Havaux and Davaud, 1994). Such stress combinations are of interest as they result in crop yield reductions and may pose a risk to plant tissues.

To examine the effect of chilling stress on the chl-E_{GSH}, chl-roGFP2-expressing plants were exposed to a low temperature (3°C) and to each of the three daily light treatments mentioned above (Figure 4); whole-plant oxidation patterns were measured every 2 h during the light period. In plants exposed to 3°C + CL, chl-roGFP2 OxD exhibited a stable state of approximately 50%, with a slight reduction after 2 h in the light period. In contrast, marked oxidation levels were observed in plants exposed to the combination of cold temperature and HL, reaching chl-roGFP2 OxD values of 60% and 80% in plants exposed to 3°C+ ML and HL, respectively, after 10 h in the light (Figure 5, A and B and Supplemental Figure S8). No decrease in OxD levels in 3°C + HL plants was observed when the light was dimmed at the end of the day. Remarkably, despite the harsh conditions, a more reduced chl-roGFP2 state was observed in newly developed leaves on the upper part of the plants, particularly near the meristem, when compared with mature leaves, throughout the day, demonstrating heterogeneous responses between old and young leaves (Figure 5, A and C). Taken together, low temperature and increasing light conditions induced extensive chl-E_{GSH} oxidation, reaching levels comparable to those measured after application of extremely high concentrations of exogenous H_2O_2 or to those observed following depletion of the GSH pool by BSO, implying a correlation between PSI photoinhibition and chl-E_{GSH} oxidation.

The demand for reduced GSH under chilling stress was also observed in transgenic tomato plants with suppressed GR activity, which demonstrated aggravated PSI photoinhibition and delayed PSI recovery (Shu et al., 2011). The extremely high roGFP2 oxidation state and the fact that no reduction was observed after returning plants to normal light conditions suggest that plants failed to acclimate to such intensive stress. The significant changes in chl-E_{GSH} (~32 mV) may indicate the induction of cell death, aligning with previously reported associations between a similar

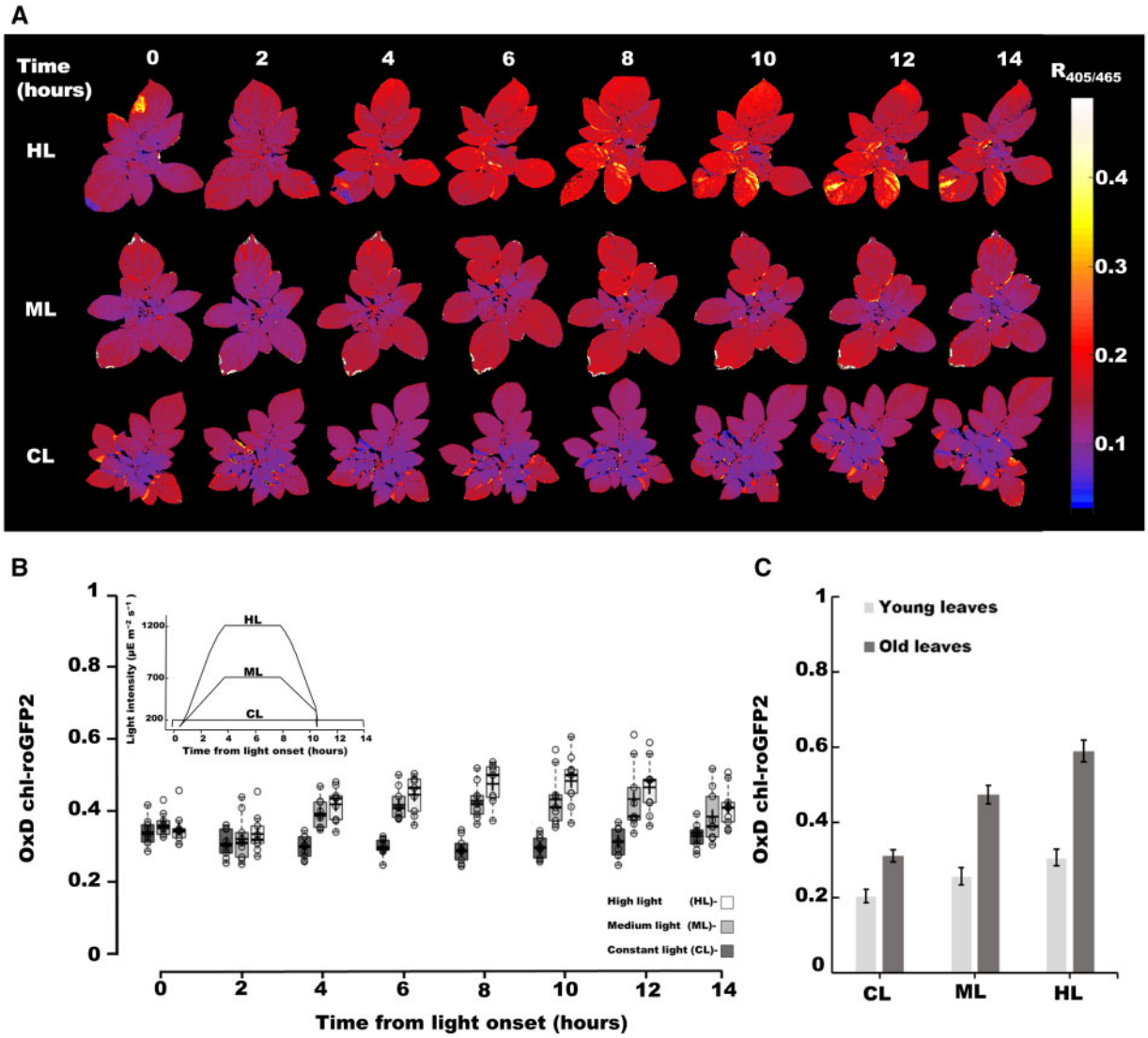

Figure 4 Daily imaging of the redox state of chl-roGFP2 under HL conditions. A, Whole-plant ratiometric images of representative potato plants at different time points during the exposure to the light regimes presented in B (inset). The color code highlights the spatial distribution of redox changes. The numbers at the top represent the time (h) from light onset. Individual plant images were digitally combined for comparison. B, Changes in chl-roGFP2 degree of oxidation (OxD) in response to changes in light intensity. Data are presented by box plots ($n = 9$). Center lines show the medians and plus signs represent sample means.; box limits indicate the 25th and 75th percentiles; whiskers extend 1.5 times the interquartile range from the 25th and 75th percentiles; open circles represent samples. Inset: daily light intensity regimes. C, Comparison between chl-roGFP2 OxD in young and old leaves 8 h from the light onset. Data present mean ± SE ($n = 9$). Raw data of fluorescence intensities measured following 405 and 465 nm excitations in chl-roGFP2-expressing and WT plants are presented in Supplemental Figure S7.

range of changes in the chloroplast and mitochondrial E_{GSH} and cell death in *Arabidopsis* and diatoms (Rosenwasser et al., 2014; Van Creveld et al., 2015; Bratt et al., 2016; Volpert et al., 2018).

Higher activity of several photoprotective mechanisms, including upregulation of energy dissipation via heat and photorespiration, in young compared with mature leaves was observed in crop plants (Bertamini and Nedunchezhian, 2003; Jiang et al., 2006). The higher reduced state of the chl-E_{GSH} in young leaves may result from their decreased photosynthetic activity, which raises the threshold at which light causes increased ROS production and subsequent chl-E_{GSH} oxidation. While the induction of these photoprotective pathways results in suboptimal photosynthetic efficiency, it may protect the photosynthetic machinery from severe destruction. Thus, the co-existence of leaves with differential chl-E_{GSH} values can be viewed as an evolutionary compromise between photosynthetic efficiency and photo-protection, enabling young leaves to better withstand unpredictable increases in light intensities and older leaves to photosynthesize more efficiently.

Drought stress initiates early oxidation of chl-E_{GSH}

Stomata closure in response to water stress restricts CO_2 diffusion and reduces the rates of Calvin–Benson cycle (CBC) reactions, resulting in higher ROS production due to

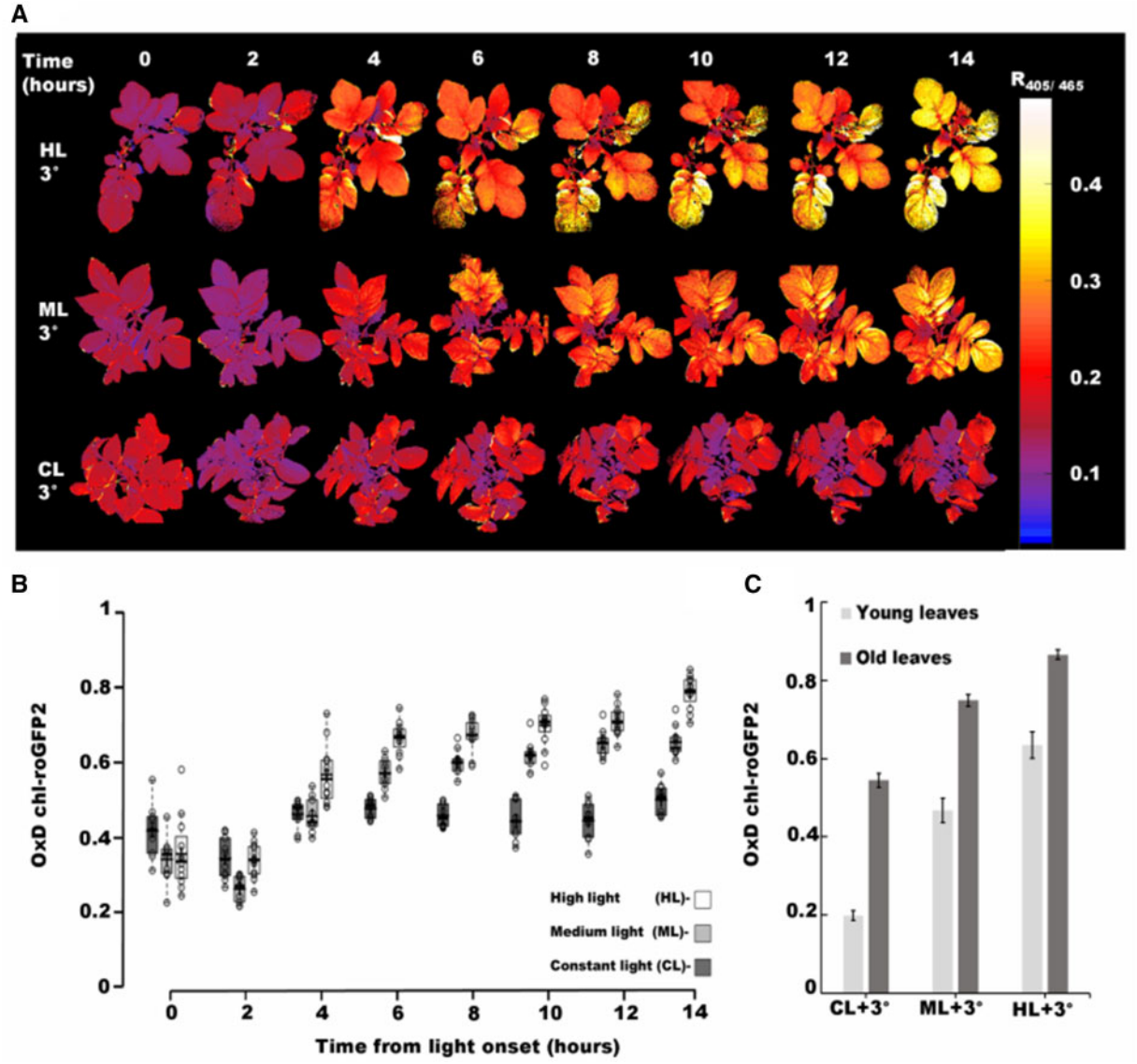

Figure 5 Combined HL and cold stress induce substantial chl-roGFP2 oxidation. Plants were exposed to the same light regime as in Figure 4, B (inset), as well as cold temperatures (3°C). A, Representative whole-plant images of potato plants over time, highlighting the spatial distribution of redox changes. The numbers at the top represent the time (h) from light onset. Individual plant images were digitally combined for comparison. B, Box plot presentation of the changes in chl-roGFP2 degree of oxidation (OxD; $n = 10–12$). Center lines show the medians and plus signs represent sample means.; box limits indicate the 25th and 75th percentiles; whiskers extend 1.5 times the interquartile range from the 25th and 75th percentiles; open circles represent samples. C, Comparison between chl-roGFP2 OxD in young versus old leaves 8 h from light onset. Data presented as mean ± SE ($n = 10–12$). Raw data of fluorescence intensities measured following 405 and 465 nm excitations in chl-roGFP2-expressing and WT plants are presented in Supplemental Figure S8.

channeling excessive light energy toward molecular oxygen (Suzuki et al., 2012). An increase in GR activity was reported under HL and water stress conditions, suggesting the increased activity of the ascorbate–GSH cycle (Yang et al., 2008; Gill and Tuteja, 2010). To explore in vivo drought-induced redox alterations in chloroplasts, chl-roGFP2 oxidation dynamics were followed during drought stress. Watering of 4-week-old plants was stopped and roGFP imaging was acquired from the third day of irrigation termination and onward. Starting from 6 d after water was withheld (Figure 6), a gradual increase in chl-roGFP2 OxD levels was noted, with oxidation initiating in the peripheral leaves, and later spreading to all plant leaves (Figure 6, A and Supplemental Figures S9, S10). No significant changes in chl-roGFP2 OxD were detected in well-watered plants during the experiment.

The rise in chl-roGFP2 OxD in water-stressed plants perfectly paralleled the decrease in carbon assimilation rates (Figure 6, B and C), pointing to the consistent relationship between photosynthetic activity and chl-E_{GSH} and suggesting that the increase in chl-E_{GSH} reflects an imbalance between light absorption and the ability to utilize it in the CBC.

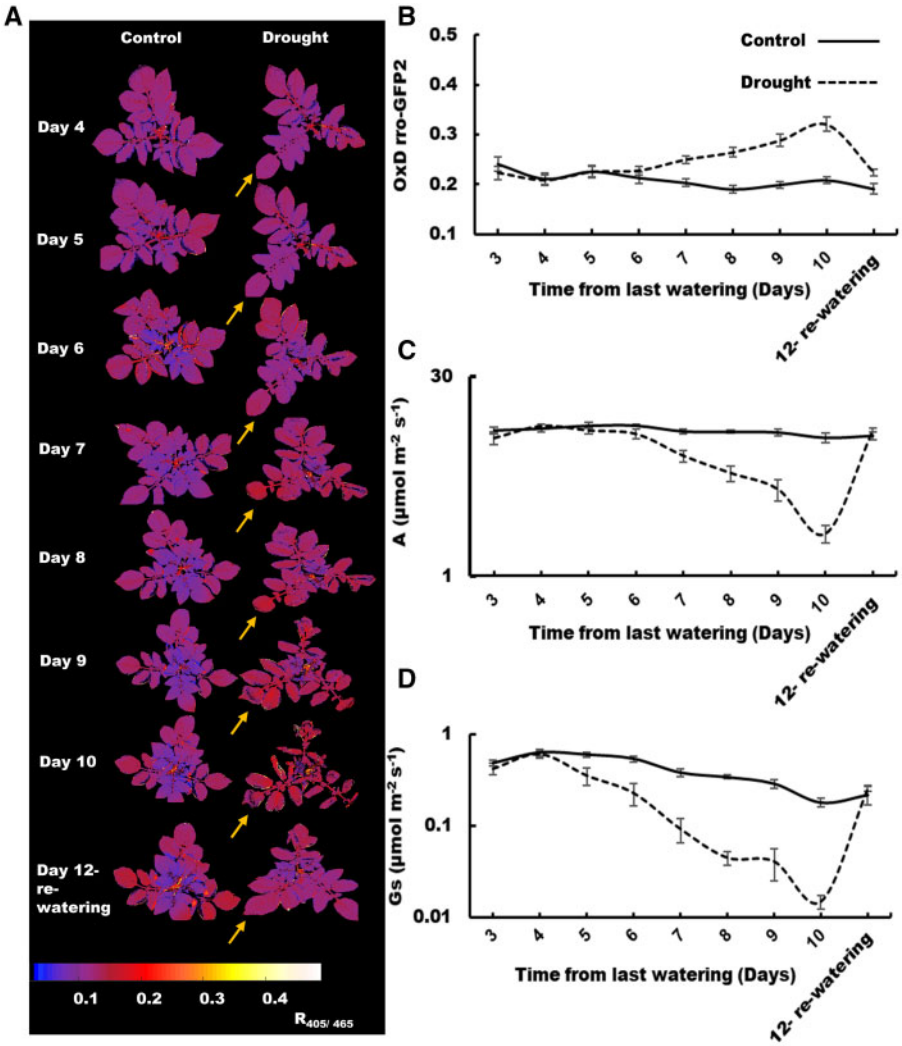

Figure 6 Changes in the redox state of chl-roGFP2 in well-watered and water-stressed plants. Drought conditions were induced by discontinuing irrigation. A, Representative whole-plant images of well-watered and water-stressed potato plants over time. The yellow arrows indicate the oxidation changes in sample leaves during water stress. The numbers at the top represent the day from irrigation termination. Individual plant images were digitally combined for comparison. Comparison between the response of young versus old leaves is shown in Supplemental Figure S10. B, OxD of roGFP2. Raw data of fluorescence intensities measured following 405 and 465 nm excitations in chl-roGFP2-expressing and WT plants are presented in Supplemental Figure S9. C, Assimilation rate (A). D, Stomatal conductance (G_S).

The decline in stomatal conductance observed 1 d before the increase in chl-roGFP2 OxD (Figure 6, B and D) further supports the notion that lower CBC activity due to a decrease in intracellular CO_2 levels resulted in an increase in chl-E_{GSH}. Steady-state redox levels and photosynthetic parameters were restored upon re-watering of water-stressed plants (Day 12), demonstrating the probe's ability to sense the reversibility of stress response. The observed increase in chl-E_{GSH} in water-stressed plants may reflect a broader increase in cellular ROS production, as suggested by the oxidation of the cytosolic and mitochondrial E_{GSH} reported for *Arabidopsis* plants (Jubany-Mari et al., 2010; Bratt et al., 2016). Future evaluations of organelle-specific changes in E_{GSH} using plant lines expressing the roGFP2 probe in various subcellular compartments will enable dissection of the exact microenvironment in which redox alterations are initiated under water stress conditions.

The GSH redox state is widely used as a marker of oxidative stress (Noctor et al., 1998; Schafer and Buettner, 2001; Dietz, 2003; Kranner et al., 2006; Meyer, 2008). Specifically, monitoring redox changes in photosynthesizing chloroplasts can provide valuable information regarding the response of leaf photosynthesis to environmental stresses. This is of great interest in crop plants in which plant productivity is greatly affected by the level of stress imposed on the photosynthetic machinery. The presented data suggest that crop plants expressing genetically encoded fluorescent sensors that report the chloroplast E_{GSH} can be a powerful tool to evaluate plant stress responses.

The presented methodology can be expanded to plant lines expressing the roGFP2 in other cellular compartments (e.g. mitochondria and peroxisomes) or other biosensors such as the roGFP2-Orp1 or iNAP, which monitor dynamic changes in H_2O_2 and NADPH, respectively (Nietzel et al.,

2019; Lim et al., 2020). Markedly, a sufficient signal-to-noise ratio is crucial to obtain reliable quantitative ratiometric images. While the bright fluorescence of the chl-roGFP2 resulted in relatively minor autofluorescence values and large dynamic range (Figure 1, D and Supplemental Figures S7–S9), working with biosensor lines exhibiting less intense fluorescence signals would require particular caution. Reasonably, a more rigorous quantitative approach for autofluorescence correction will be needed. As demonstrated for confocal microscopy analysis, assessing the structured autofluorescence, typically observed in plant tissues in response to 405 nm excitation, can be achieved by recording emissions at 435–485 nm. Then, correction for the autofluorescence bleed-through into one of the biosensor channels can be achieved by subtracting a scaled version of the autofluorescence image from the biosensor image (Fricker, 2016). Similar corrections may provide high-quality whole-plant ratiometric images, even for plant lines exhibiting dim fluorescence signals.

The applications of the presented whole-plant redox imaging methodology can be broad, including, for example, in testing the performance of various chemicals in improving plant tolerance under stress conditions. Plant lines expressing genetically encoded biosensors can also be applied to improve high-throughput plant phenotyping in plant breeding programs and ultimately serve as highly sensitive tools for early detection of stress responses in the field. Notably, the need for highly sensitive fluorescence cameras may limit the accessibility of this technology, raising the need to develop portable and sensitive instruments to monitor fluorescence signals in the field. Taken together, given the significant role of redox metabolism in plant acclimation to stress conditions, crop plants expressing redox sensors can expand the basic understanding of plant stress physiology and extend the arsenal of early noninvasive tools for detection of stress-induced physiological changes in crops.

Materials and methods

Plant material, growth conditions, and experimental setup

Wild-type and chl-roGFP2-expressing potato (*S. tuberosum*) plants were planted in moist soil in 26.82 × 53.49 cm pots and placed in a controlled-environment greenhouse. Plants were vegetatively propagated from cuttings. All experiments were performed on 3–4-week-old plants in a FytoScope FS-RI 1600 plant growth chamber (Photon Systems Instruments). Plants were moved to the chamber several days before the experiments to allow acclimation to the chamber environment. In all experiments, plants were incubated in 60%–70% relative humidity (RH) and ambient CO_2.

Production of transgenic plants

Potato leaves (cv Désirée) were used for *Agrobacterium*-mediated infection, as previously described (Ooms et al., 1987; Teper Bamnolker et al., 2017). Leaves were taken from clean culture and infected by *Agrobacterium tumefaciens* strain LBA 4404 harboring the pART27 plasmid, which contains the chl-roGFP2 construct (Haber et al., 2021). After the inoculation, cultures were transferred to cali induction medium containing kanamycin 50 (mg/L), cefotaxime 500 (mg/L), 6-benzylaminopurine (BAP) 0.1 mg/L, and 1-naphthaleneacetic acid (NAA) 5 mg/L, for 10 d. Then, plants were transferred to shot induction medium (regeneration medium) containing zeatin-riboside (ZR) 2 mg/L, NAA 0.02 mg/L gibberellic acid 3 GA3 0.02 mg/L, and appropriate antibiotics. Medium was refreshed every 14 d until shoots appeared. Transgenic explants from cultures that were fully regenerated with no roots were transferred to moist soil for rooting and sorting. Appropriate lines were selected by evaluating the chl-roGFP2 fluorescence signal (Supplemental Figure S1).

Confocal microscopy

Images were acquired with Leica DMI4000 confocal system (Leica Microsystems) and the LAS X Life Science Software, while using HCX APO U-V-I 40×/0.75 DRY UV objective. Images were acquired at a 4096 × 4096-pixel resolution, with a 507–534 nm emission bandpass and PMT gain of −628.2(V) following excitation at 488 or 405 nm for chl-roGFP2 fluorescence detection. For those images, 15% and 30% of the maximum laser intensity were used for 488 and 405 nm excitation, respectively. A 652–692 nm emission bandpass and PMT gain of −571.4(V) following excitation at 488 nm were used to image chlorophyll fluorescence. Autofluorescence following excitation at 405 nm was recorded at 431–469 nm. Merged images were generated using Fiji software. Background subtraction of confocal images was conducted by subtracting the mean value of a user-defined region of interest (ROI) that did not include chloroplasts and pixel-by-pixel subtraction of autofluorescence values from the 405 nm image. The ratiometric images were created by dividing, pixel by pixel, the 405 nm image by the 465 nm image, and displaying the result in false colors using Matlab.

Gas exchange measurements

Carbon assimilation measurements were made using the portable gas analyzer Li-Cor-6800 gas exchange (LICOR, Lincoln, NE, USA).

The leaf chamber was set to maintain a constant CO_2 level of 400 ppm. Light intensities were similar to those applied in the growing chamber. The temperature and humidity were set at 25°C and 70%. Net photosynthesis (A) and stomatal conductance to water vapor (Gs) were measured. Between 6 and 9 plants were randomly selected for each treatment and measurements were taken at 12 PM each day.

Chl-roGFP2 fluorescence measurements and image analysis

Whole-plant chl-roGFP2 fluorescence was detected using an Advanced Molecular Imager HT (Spectral Ami-HT, Spectral Instruments Imaging, LLC., USA), and images were acquired using the AMIview software. For chl-roGFP2 fluorescence

detection, excitation was performed with 405 nm ± 10 or 465 nm ± 10 LED light sources and a 515 nm ± 10 emission filter was used. For chlorophyll detection, a 405 nm ± 10 LED light source and a 670 nm ± 10 emission filter were used. All images were taken under the following settings: exposure time = 1 s, pixel binning = 2, field of view (FOV) = 25 cm, and LED excitation power 40% and 60%, for 405 and 465 nm excitations, respectively. Excitation power for chlorophyll detection was 5%. Chlorophyll autofluorescence was measured to generate a chlorophyll mask, which was then used to select pixels that returned a positive chlorophyll fluorescence signal. Only those pixels were subsequently considered for the roGFP analysis. For background correction, the average signal of wild-type plants without chl-roGFP2 was determined and subtracted from the values detected in the chl-roGFP2 fluorescence signals. Ratiometric images were created by dividing, pixel by pixel, the 405 nm image by the 465 nm image, and displaying the result in false colors. Images were preprocessed using a custom-written Matlab script.

For calibration of the probe response, detached, fully expanded leaves were immersed in 1 M H_2O_2 or 100 mM DTT, and ratiometric images for fully oxidized and fully reduced states, respectively, were then acquired. roGFP2 OxD (the relative quantity of oxidized roGFP proteins) was calculated for individual plants based on the whole-plant fluorescence signal, according to Equation (1) (Meyer et al., 2007)

$$\mathrm{OxD}_{\mathrm{roGFP2}} = \frac{R - R_{\mathrm{red}}}{(I_{465\mathrm{min}}/I_{465\mathrm{max}})(R_{\mathrm{ox}} - R) + (R - R_{\mathrm{red}})},$$

where R represents the 405/465 fluorescence ratio at the indicated time and treatment, R_{red} the 405/465 fluorescence ratio under fully reduced conditions, R_{ox} the 405/465 fluorescence ratio under fully oxidized conditions, $I_{465\mathrm{ox}}$ the fluorescence emitted at 515 nm when excited at 465 nm under fully oxidized conditions, and $I_{480\mathrm{red}}$ the fluorescence emitted at 515 nm when excited at 465 nm under fully reduced conditions. E_{GSH} values were calculated according to Schwarzländer et al. (2008). Box plots were created using the BoxPlotR tool (Spitzer et al., 2014).

Supplemental data

The following materials are available in the online version of this article.

Supplemental Figure S1. Schematic steps of *S. tuberosum* "Desiree" transformation.

Supplemental Figure S2. Comparison of chl-roGFP2 ratio values under steady-state conditions in three independent lines expressing chl-roGFP2 in the chloroplast stroma.

Supplemental Figure S3. Whole-plant imaging of WT and transgenic plant expressing roGFP2 in the chloroplast.

Supplemental Figure S4. Pixel distribution analysis of plants watered with H_2O_2.

Supplemental Figure S5. Pixel distribution analysis of plants watered with buthionine sulfoximine (BSO).

Supplemental Figure S6. Pixel distribution analysis of leaves treated with various H_2O_2 concentrations.

Supplemental Figure S7. Fluorescence intensity of chl-roGFP2 and WT plants under HL.

Supplemental Figure S8. Fluorescence intensity of chl-roGFP2 and WT plants under HL and cold stress (3°).

Supplemental Figure S9. Fluorescence intensity of chl-roGFP2 and WT plants under different water regimes.

Supplemental Figure S10. Comparison between chl-roGFP2 OxD in young versus old leaves on Day 10 of the drought experiments.

Supplemental Movie S1. Whole-plant redox imaging of a potato plant watered with H_2O_2.

Acknowledgments

The authors thank Andreas J. Meyer for his critical comments on the manuscript. They thank Dani Eshel and Paula Teper-Bemnolker for providing the starting materials and protocol for potato transformation.

Funding

This research was supported by the Israel Science Foundation (grant No. 826/17 and No. 827/17) to SR.

Author contributions

M.H. and S.R. conceived and designed the research. M.H., N.L., E.Z., O.B and D.W. performed the research. M.H. and S.R. analyzed the data. M.H. and S.R. wrote the manuscript.

Conflict of interest statement. The authors have no conflicts of interest to declare.

References

Albrecht SC, Barata AG, Großhans J, Teleman AA, Dick TP (2011) In vivo mapping of hydrogen peroxide and oxidized glutathione reveals chemical and regional specificity of redox homeostasis. Cell Metab **14:** 819–829

Bach S, Yada RY, Bizimungu B, Sullivan JA (2012) Genotype by environment interaction effects on fibre components in potato (*Solanum tuberosum L.*). Euphytica **187:** 77–86

Bertamini M, Nedunchezhian N (2003) Photoinhibition of photosynthesis in mature and young leaves of grapevine (*Vitis vinifera* L.). Plant Sci **164:** 635–644

Bohnert HJ (2007) Abiotic stress. eLS

Born N, Behringer D, Liepelt S, Beyer S, Schwerdtfeger M, Ziegenhagen B, Koch M (2014) Monitoring plant drought stress response using terahertz time-domain spectroscopy. Plant Physiol **164:** 1571

Bratt A, Rosenwasser S, Meyer A, Fluhr R (2016) Organelle redox autonomy during environmental stress. Plant Cell Environ **39:** 1909–1919

Van Breusegem F, Bailey-Serres J, Mittler R (2008) Unraveling the tapestry of networks involving reactive oxygen species in plants. Plant Physiol **147:** 978–984

Burlingame B, Mouillé B, Charrondiére R (2009) Nutrients, bioactive non-nutrients and anti-nutrients in potatoes. J Food Compost Anal **22:** 494–502

Costa JM, Grant OM, Chaves MM (2013) Thermography to explore plant–environment interactions. J Exp Bot **64:** 3937–3949

Van Creveld SG, Rosenwasser S, Schatz D, Koren I, Vardi A (2015) Early perturbation in mitochondria redox homeostasis in response to environmental stress predicts cell fate in diatoms. ISME J **9:** 385–395

Deblonde PMK, Ledent J-F (2001) Effects of moderate drought conditions on green leaf number, stem height, leaf length and tuber yield of potato cultivars. Eur J Agron **14:** 31–41

Devaux A, Kromann P, Ortiz O (2014) Potatoes for sustainable global food security. Potato Res **57:** 185–199

Dietz K-J (2003) Redox control, redox signaling, and redox homeostasis in plant cells. Int Rev Cytol **228:** 141–193

Dooley CT, Dore TM, Hanson GT, Jackson WC, Remington SJ, Tsien RY (2004) Imaging dynamic redox changes in mammalian cells with green fluorescent protein indicators. J Biol Chem **279:** 22284–22293

Exposito-Rodriguez M, Laissue PP, Yvon-Durocher G, Smirnoff N, Mullineaux PM (2017) Photosynthesis-dependent H_2O_2 transfer from chloroplasts to nuclei provides a high-light signalling mechanism. Nat Commun **8:** 49

Fahad S, Bajwa AA, Nazir U, Anjum SA, Farooq A, Zohaib A, Sadia S, Nasim W, Adkins S, Saud S (2017) Crop production under drought and heat stress: plant responses and management options. Front Plant Sci **8:** 1147

da FAOSTAT E (2014) Disponível em: http://wwwfao.org/. faostat/en/#home

Fichman Y, Miller G, Mittler R (2019) Whole-plant live imaging of reactive oxygen species. Mol Plant **12:** 1203–1210

Fichman Y, Zandalinas SI, Sengupta S, Burks D, Myers RJ, Azad RK, Mittler R (2020) MYB30 orchestrates systemic reactive oxygen signaling and plant acclimation. Plant Physiol **184:** 666–675

Fichman Y, Mittler R (2021) A systemic whole-plant change in redox levels accompanies the rapid systemic response to wounding. Plant Physiol **186**: 4–8

Fricker MD (2016) Quantitative redox imaging software. Antioxid Redox Signal **24:** 752–762.

Foyer CH, Noctor G (2003) Redox sensing and signalling associated with reactive oxygen in chloroplasts, peroxisomes and mitochondria. Physiol Plant **119:** 355–364

Gadjev I, Vanderauwera S, Gechev TS, Laloi C, Minkov IN, Shulaev V, Apel K, Inzé D, Mittler R, Van Breusegem F (2006) Transcriptomic footprints disclose specificity of reactive oxygen species signaling in Arabidopsis. Plant Physiol **141:** 436–445

Gao Q, Zhang L (2008) Ultraviolet-B-induced oxidative stress and antioxidant defense system responses in ascorbate-deficient vtc1 mutants of *Arabidopsis thaliana*. J Plant Physiol **165:** 138–148

George TS, Taylor MA, Dodd IC, White PJ (2017) Climate change and consequences for potato production: a review of tolerance to emerging abiotic stress. Potato Res **60:** 239–268.

Gill SS, Tuteja N (2010) Reactive oxygen species and antioxidant machinery in abiotic stress tolerance in crop plants. Plant Physiol Biochem **48:** 909–930

Gutscher M, Pauleau A-L, Marty L, Brach T, Wabnitz GH, Samstag Y, Meyer AJ, Dick TP (2008) Real-time imaging of the intracellular glutathione redox potential. Nat Methods **5:** 553–559

Haber Z, Lampl N, Meyer AJ, Zelinger E, Hipsch M, Rosenwasser S (2021) Resolving diurnal dynamics of the chloroplastic glutathione redox state in Arabidopsis reveals its photosynthetically-derived oxidation. Plant Cell (doi: 10.1093/plcell/koab068)

Halliwell B, Whiteman M (2004) Measuring reactive species and oxidative damage in vivo and in cell culture: how should you do it and what do the results mean. Br J Pharmacol **142:** 231–255

Hanson GT, Aggeler R, Oglesbee D, Cannon M, Capaldi RA, Tsien RY, Remington SJ (2004) Investigating mitochondrial redox potential with redox-sensitive green fluorescent protein indicators. J Biol Chem **279:** 13044–13053

Havaux M, Davaud A (1994) Photoinhibition of photosynthesis in chilled potato leaves is not correlated with a loss of Photosystem-II activity. Photosynth Res **40:** 75–92

Jiang C-D, Gao H-Y, Zou Q, Jiang G-M, Li L-H (2006) Leaf orientation, photorespiration and xanthophyll cycle protect young soybean leaves against high irradiance in field. Environ Exp Bot **55:** 87–96

Jiang K, Schwarzer C, Lally E, Zhang S, Ruzin S, Machen T, Remington SJ, Feldman L (2006) Expression and characterization of a redox-sensing green fluorescent protein (reduction–oxidation–sensitive green fluorescent protein) in Arabidopsis. Plant Physiol **141:** 397–403

Jubany-Mari T, Alegre-Batlle L, Jiang K, Feldman LJ (2010) Use of a redox-sensing GFP (c-roGFP1) for real-time monitoring of cytosol redox status in *Arabidopsis thaliana* water-stressed plants. FEBS Lett **584:** 889–897

König J, Baier M, Horling F, Kahmann U, Harris G, Schürmann P, Dietz K-J (2002) The plant-specific function of 2-Cys peroxiredoxin-mediated detoxification of peroxides in the redox-hierarchy of photosynthetic electron flux. Proc Natl Acad Sci USA **99:** 5738–5743

Kranner I, Birtić S, Anderson KM, Pritchard HW (2006) Glutathione half-cell reduction potential: a universal stress marker and modulator of programmed cell death. Free Radic Biol Med **40:** 2155–2165

Lew TTS, Koman VB, Silmore KS, Seo JS, Gordiichuk P, Kwak S-Y, Park M, Ang MC-Y, Khong DT, Lee MA, et al. (2020) Real-time detection of wound-induced H_2O_2 signalling waves in plants with optical nanosensors. Nat Plants **6:** 404–415

Meyer AJ (2008) The integration of glutathione homeostasis and redox signaling. J Plant Physiol **165:** 1390–1403

Meyer AJ, Brach T, Marty L, Kreye S, Rouhier N, Jacquot J, Hell R (2007) Redox-sensitive GFP in *Arabidopsis thaliana* is a quantitative biosensor for the redox potential of the cellular glutathione redox buffer. Plant J **52:** 973–986

Meyer AJ, Dick TP (2010) Fluorescent protein-based redox probes. Antioxid Redox Signal **13:** 621–650

Lim SL, Voon CP, Guan X, Yang Y, Gardeström P, Lim BL (2020) In planta study of photosynthesis and photorespiration using NADPH and NADH/NAD+ fluorescent protein sensors. Nat Commun **11:** 3238

Miller GAD, Suzuki N, Ciftci-Yilmaz S, Mittler RON (2010) Reactive oxygen species homeostasis and signalling during drought and salinity stresses. Plant Cell Environ **33:** 453–467

Møller IM, Sweetlove LJ (2010) ROS signalling—specificity is required. Trends Plant Sci **15:** 370–374

Nietzel T, Elsässer M, Ruberti C, Steinbeck J, Ugalde JM, Fuchs P, Wagner S, Ostermann L, Moseler A, Lemke P, et al. (2019) The fluorescent protein sensor roGFP2-Orp1 monitors in vivo H_2O_2 and thiol redox integration and elucidates intracellular H_2O_2 dynamics during elicitor-induced oxidative burst in Arabidopsis. New Phytol **221:** 1649–1664

Noctor G, Arisi A-CM, Jouanin L, Kunert KJ, Rennenberg H, Foyer CH (1998) Glutathione: biosynthesis, metabolism and relationship to stress tolerance explored in transformed plants. J Exp Bot **49:** 623–647

Ooms G, Burrell MM, Karp A, Bevan M, Hille J (1987) Genetic transformation in two potato cultivars with T-DNA from disarmed Agrobacterium. Theor Appl Genet **73:** 744–750

Rosenwasser S, van Creveld SG, Schatz D, Malitsky S, Tzfadia O, Aharoni A, Levin Y, Gabashvili A, Feldmesser E, Vardi A (2014) Mapping the diatom redox-sensitive proteome provides insight into response to nitrogen stress in the marine environment. Proc Natl Acad Sci USA **111:** 2740–2745

Rosenwasser S, Rot I, Meyer AJ, Feldman L, Jiang K, Friedman H (2010) A fluorometer-based method for monitoring oxidation of redox-sensitive GFP (roGFP) during development and extended dark stress. Physiol Plant **138:** 493–502

Schafer FQ, Buettner GR (2001) Redox environment of the cell as viewed through the redox state of the glutathione disulfide/glutathione couple. Free Radic Biol Med **30:** 1191–1212

Schwarzländer M, Dick TP, Meyer AJ, Morgan B (2016) Dissecting redox biology using fluorescent protein sensors. Antioxid Redox Signal **24:** 680–712

Schwarzländer M, Fricker MD, Müller C, Marty L, Brach T, Novak J, Sweetlove LJ, Hell R, Meyer AJ (2008) Confocal imaging of glutathione redox potential in living plant cells. J Microsc **231:** 299–316

Shu DF, Wang LY, Duan M, Deng YS, Meng QW (2011) Antisense-mediated depletion of tomato chloroplast glutathione reductase enhances susceptibility to chilling stress. Plant Physiol Biochem **49:** 1228–1237

Spitzer M, Wildenhain J, Rappsilber J, Tyers M (2014) BoxPlotR: a web tool for generation of box plots. Nat Methods **11:** 121

Suzuki N, Koussevitzky S, Mittler RON, Miller GAD (2012) ROS and redox signalling in the response of plants to abiotic stress. Plant Cell Environ **35:** 259–270

Teper Bamnolker P, Buskila Y, Belausov E, Wolf D, Doron Faigenboim A, Ben Dor S, Van der Hoorn RAL, Lers A, Eshel D (2017) Vacuolar processing enzyme activates programmed cell death in the apical meristem inducing loss of apical dominance. Plant Cell Environ **40:** 2381–2392

Ugalde JM, Fuchs P, Nietzel T, Cutolo E, Homagk M, Vothknecht UC, Holuigue L, Schwarzländer M, Müller-Schüssele SJ, Meyer AJ (2020) Chloroplast-derived photo-oxidative stress causes changes in H_2O_2 and E_{GSH} in other subcellular compartments. Plant Physiol **186**: 125–141

Volpert A, Graff van Creveld S, Rosenwasser S, Vardi A (2018) Diurnal fluctuations in chloroplast GSH redox state regulate susceptibility to oxidative stress and cell fate in a bloom-forming diatom. J Phycol **54:** 329–341

Wang H, Qian X, Zhang L, Xu S, Li H, Xia X, Dai L, Xu L, Yu J, Liu X (2018) A method of high throughput monitoring crop physiology using chlorophyll fluorescence and multispectral imaging. Front Plant Sci **9:** 407

Wu H, Nißler R, Morris V, Herrmann N, Hu P, Jeon S-J, Kruss S, Giraldo JP (2020) Monitoring plant health with near-infrared fluorescent H_2O_2 nanosensors. Nano Lett **20:** 2432–2442

Yang Y, Han C, Liu Q, Lin B, Wang J (2008) Effect of drought and low light on growth and enzymatic antioxidant system of *Picea asperata* seedlings. Acta Physiol Plant **30:** 433–440

Zhang S, Zhao X, Niu H, Shi Y, Cai Y, Jiang G (2009) Superparamagnetic Fe_3O_4 nanoparticles as catalysts for the catalytic oxidation of phenolic and aniline compounds. J Hazard Mater **167:** 560–566

Zhu J-K (2016) Abiotic stress signaling and responses in plants. Cell **167:** 313–324